# Probing hard/soft factorization via beam-spin asymmetry in exclusive pion electroproduction from the proton

A.C. Postuma[a], G.M. Huber[a], D. Gaskell[b], N. Heinrich[a], T. Horn[c,b], M. Junaid[a], S.J.D. Kay[a,d], V. Kumar[a], P. Markowitz[e], J. Roche[f], R. Trotta[c], A. Usman[a], B.-G. Yu[g], T.K. Choi[h], K.-J. Kong[g], S. Ali[c], R. Ambrose[a], D. Androic[i], W. Armstrong[j,k], A. Bandari[l], V. Berdnikov[c], H. Bhatt[m], D. Bhetuwal[m], D. Biswas[n], M. Boer[n], P. Bosted[l], E. Brash[o], A. Camsonne[b], J.P. Chen[b], J. Chen[l], M. Chen[r], M.E. Christy[p], S. Covrig[b], M. M. Dalton[b], W. Deconinck[u], M. Diefenthaler[b], B. Duran[j], D. Dutta[m], M. Elaasar[v], R. Ent[b], H. Fenker[b], E. Fuchey[w], D. Hamilton[x], J.-O. Hansen[b], F. Hauenstein[y], S. Jia[j], M.K. Jones[b], S. Joosten[k], M.L. Kabir[m], A. Karki[m], C. Keppel[b], E. Kinney[z], N. Lashley-Colthirst[p], W.B. Li[ac], D. Mack[b], S. Malace[b], M. McCaughan[b], Z.E. Meziani[k,j], R. Michaels[b], R. Montgomery[x], M. Muhoza[c], C. Muñoz Camacho[aa], G. Niculescu[t], I. Niculescu[t], Z. Papandreou[a], S. Park[ac], E. Pooser[b], M. Rehfuss[j], B. Sawatzky[b], G.R. Smith[b], H. Szumila-Vance[b], A. Teymurazyan[a], H. Voskanyan[ab], B. Wojtsekhowski[b], S.A. Wood[b], Z. Ye[k], C. Yero[e], J. Zhang[r], X. Zheng[r]

[a]*University of Regina, Regina, S4S 0A2, SK, Canada*
[b]*Thomas Jefferson National Accelerator Facility, Newport News, 23606, Virginia, USA*
[c]*Catholic University of America, Washington, 20064, DC, USA*
[d]*University of York, Heslington, YO10 5DD, York, United Kingdom*
[e]*Florida International University, University Park, 33199, Florida, USA*
[f]*Ohio University, Athens, 45701, Ohio, USA*
[g]*Research Institute of Basic Sciences, Korea Aerospace University, Goyang, 10540, Korea*
[h]*Department of Physics, Yonsei University, Wonju, 26493, Korea*
[i]*University of Zagreb, Zagreb, 10000, Croatia*
[j]*Temple University, Philadelphia, 19122, Pennsylvania, USA*
[k]*Argonne National Laboratory, Lemont, 60439, Illinois, USA*
[l]*College of William & Mary, Williamsburg, 23185, Virginia, USA*
[m]*Mississippi State University, Mississippi State, 39762, Mississippi State, USA*
[n]*Virginia Tech, Blacksburg, 24061, Virginia, USA*
[o]*Christopher Newport University, Newport News, 23606, Virginia, USA*
[p]*Hampton University, Hampton, 23669, Virginia, USA*
[q]*University of Tennessee, Knoxville, 37996, Tennessee, USA*
[r]*University of Virginia, Charlottesville, 22903, Virginia, USA*
[s]*University of New Hampshire, Durham, 03824, New Hampshire, USA*
[t]*James Madison University, Harrisonburg, 22807, Virginia, USA*
[u]*University of Manitoba, Winnipeg, R3T 2N2, Manitoba, Canada*
[v]*Southern University at New Orleans, New Orleans, 70126, Louisiana, USA*
[w]*University of Conneticut, Storrs, 06269, Conneticut, USA*
[x]*University of Glasgow, Glasgow, G12 8QQ, United Kingdom*
[y]*Old Dominion University, Norfolk, 23529, Virginia, USA*
[z]*University of Colorado, Boulder, 80309, Colorado, USA*
[aa]*Universite Paris-Saclay, CNRS, IJCLab, Orsay, 91406, France*
[ab]*A.I. Alikhanyan National Science Laboratory (Yerevan Physics Institute), Yerevan, 0036, Armenia*
[ac]*Stony Brook University, , Stony Brook, 11794, New York, USA*

**Abstract**

Deep exclusive meson production (DEMP) reactions, such as $p(\vec{e}, e'\pi^+)n$, provide opportunities to study the three-dimensional structure of the nucleon through differential cross section and beam- and target-spin asymmetry measurements. This work aims to probe the onset of the hard/soft factorization regime through the exclusive $p(\vec{e}, e'\pi^+)n$ reaction, as measured in the KaonLT experiment at Jefferson Lab Hall C. A 10.6 GeV longitudinally polarized electron beam was incident on an unpolarized liquid hydrogen target, and the scattered electron and produced meson were detected in two magnetic focusing spectrometers, enabling precision cross section measurements. The cross section ratio $\sigma_{LT'}/\sigma_0$ was extracted from the beam-spin asymmetry $A_{LU}$. The $t$-dependence of $\sigma_{LT'}/\sigma_0$ was determined at fixed $Q^2$ and $x_B$ over a range of kinematics from $2 < Q^2 < 6$ GeV$^2$ above the resonance region ($W > 2$ GeV). Furthermore, these data are combined with recent results from CLAS/CLAS12 to determine the $Q^2$-dependence of $\sigma_{LT'}/\sigma_0$ at two ($x_B$, $t$) settings. This was fairly flat, with $Q^2$ not having a measurable effect on the value of $\sigma_{LT'}/\sigma_0$ in the range explored. Results are compared to predictions from the generalized parton distribution (GPD) formalism, which relies explicitly on hard/soft factorization, and Regge formalism. The Regge models better predict $\sigma_{LT'}/\sigma_0$, which implies that the factorization regime is not yet reached.

*Keywords:* Deep Exclusive Meson Production, hadron structure, Beam-Spin Asymmetry, hard/soft factorization, Generalized Parton Distributions

## 1. Introduction

A quantitative description of simple hadronic systems such as light mesons and nucleons is essential to our understanding of nuclear matter. Deep exclusive meson production (DEMP) reactions, such as $p(\vec{e}, e'\pi^+)n$, provide opportunities to study the three-dimensional structure of the nucleon through differential cross section and beam- and target-spin asymmetry measurements. DEMP reactions can be conveniently described using three Lorentz invariants. $Q^2 = -(p_e - p_{e'})^2$ is the negative of the four-momentum transfer squared of the virtual photon. Additionally, the reaction is characterized by the invariant mass of the virtual photon-nucleon system, $W = (p_p + p_{\gamma^*})^2$, and the Mandelstam variable $t = (p_{\gamma^*} - p_\pi)^2$. Alternatively, the Bjorken scaling variable $x_B = Q^2/(2p_p \cdot p_{\gamma^*})$ may replace $W$.

Hard/soft factorization describes the expression of the $\gamma^* p$ amplitude as the convolution of a hard-scattering subprocess and a non-perturbative (soft) subprocess. A factorization theorem has been proven for DEMP events involving longitudinally polarized virtual photons [1, 2], and the contribution of transversely polarized virtual photons has been treated as a twist-3 effect in this approach [3]. Hard/soft factorization is expected to apply in the limit of large $Q^2$ at fixed $x_B$ and $t$. For Deep Virtual Compton Scattering (DVCS), factorization appears valid even at modest $Q^2 \approx 2$ GeV$^2$ [4, 5], but the minimum $Q^2$ for which factorization may be valid for DEMP is still unknown [6].

The identification of this factorization regime for $p(\vec{e}, e'\pi^+)n$ is of high interest to hadronic physics, as factorization allows for the extraction of Generalized Parton Distributions (GPDs). GPDs [7, 8] unify the concepts of parton distributions and hadronic form factors by correlating the transverse position and longitudinal momentum of partons. Measuring these observables is expected to facilitate numerous advances in our understanding of nucleon structure, for example providing information on the orbital angular momentum of partons, which is needed for solving the proton spin crisis [8]. DEMP reactions provide complementary information to DVCS towards the extraction of GPDs; DVCS primarily probes chiral-even GPDs, whereas DEMP also probes chiral-odd GPDs [9]. The DEMP reaction $p(\vec{e}, e'\pi^+)n$ in particular has a significant contribution from the GPD $H_T$ [3], therefore polarized $\pi^+$ observables in the factorization regime could be used to probe fundamental quantities such as the still unknown tensor charge of the nucleon, which is calculated from the integral of $H_T$ [9].

To investigate the onset of hard/soft factorization, the KaonLT experiment (E12-09-011 [10]) at Hall C of the Thomas Jefferson National Accelerator Facility (Jefferson Lab or JLab) measured DEMP reactions over a range of kinematics from $2 < Q^2 < 6$ GeV$^2$ above the resonance region ($W > 2$ GeV). The KaonLT data will allow for the extraction of a number of hadronic structure observables including the total cross section $\sigma_0$, longitudinal and transverse cross sections $\sigma_L$ and $\sigma_T$ (where the subscript denotes the virtual photon polarization), and interference cross sections $\sigma_{LT}$, $\sigma_{TT}$, and $\sigma_{LT'}$.

In this work, the cross section ratio $\sigma_{LT'}/\sigma_0$ is extracted from beam-spin asymmetry measurements of $p(\vec{e}, e'\pi^+)n$. The prime in the subscript of $\sigma_{LT'}$ denotes polarization, as $\sigma_{LT'}$ is only accessible in the case of a longitudinally polarized incident electron beam. $\sigma_{LT'}$ is proportional to the imaginary part of interference between longitudinally and transversely polarized virtual photons (as opposed to $\sigma_{LT}$, which is accessible with an unpolarized beam, and is proportional to the real part of the same interference amplitude) [11]. In the one-photon exchange approximation, this asymmetry can be expressed as [11, 12]

$$A_{LU}(Q^2, x_B, t, \phi) = \frac{\sqrt{2\epsilon(1-\epsilon)}\frac{\sigma_{LT'}}{\sigma_0}\sin\phi}{1 + \sqrt{2\epsilon(1+\epsilon)}\frac{\sigma_{LT}}{\sigma_0}\cos\phi + \epsilon\frac{\sigma_{TT}}{\sigma_0}\cos 2\phi}, \quad (1)$$

where $\epsilon$ is the ratio of longitudinal and transverse virtual photon polarization and $\phi$ is the azimuthal angle shown in Fig. 1 [13]. All three interference terms are required to vanish when $t = -|t|_{\min}$ and $t = -|t|_{\max}$; for these values the $\gamma^* p \to \pi^+ n$ reaction is collinear in the struck proton rest system and $\phi$ is undefined. The subscript $LU$ specifies the asymmetry resulting from a longitudinally polarized incident electron beam and an unpolarized target. $\sigma_{LT'}/\sigma_0$ is extracted from the asymmetry via the $\sin\phi$ amplitude of $A_{LU}$, defined as $A_{LU}^{\sin\phi} = \sqrt{2\epsilon(1-\epsilon)}\sigma_{LT'}/\sigma_0$.

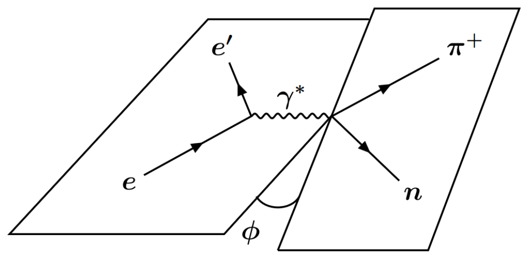


Figure 1: Reaction diagram for $p(\vec{e}, e'\pi^+)n$. The angle $\phi$ is defined as the azimuthal angle between the electron scattering plane (defined by $e$ and $e'$) and the hadron reaction plane (defined by $\pi^+$ and $n$).

There are two main approaches to describe this observable: the first is to assume factorization and describe the reaction

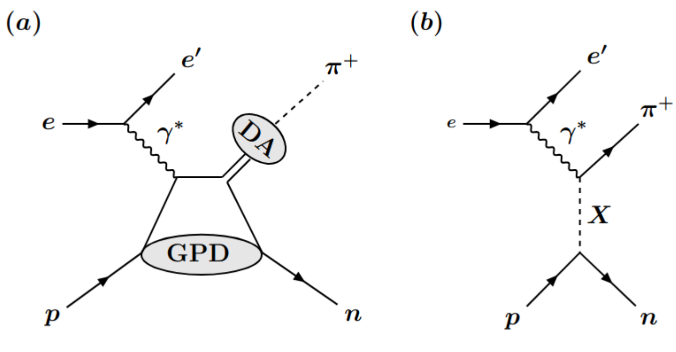


Figure 2: Exclusive $\pi^+$ electroproduction from the proton. (a) Factorization of the reaction into a hard scattering part and a soft part described by a GPD. An additional soft part known as the pion distribution amplitude (DA) describes the final state pion formation. (b) A Regge process, in which $X$ represents the exchange of several particles along a Regge trajectory up to a cutoff.

using GPDs (Fig. 2(a)). An alternative description of DEMP reactions is based on Regge models. Here, the interaction is mediated by the exchange of meson trajectories in the $t$ channel (Fig. 2(b)). Regge models [14] have been extended from photoproduction ($Q^2$=0) [15] to DEMP [16], and have successfully described DEMP reactions at Hall C kinematics [17]. Unlike GPDs, the validity of Regge models does not explicitly rely on hard/soft factorization, neither do they describe the three-dimensional structure of the nucleon. This work compares $\sigma_{LT'}/\sigma_0$ to predictions from three models [18, 15, 19] to explore if a GPD or Regge description is more applicable to DEMP reactions at these kinematics. If the GPD-based model clearly outperforms the Regge models, it would be a strong indication of factorization validity at these kinematics.

## 2. Experiment

$A_{LU}$ is experimentally calculated as a fractional difference of yield based on the helicity of the incident electron $Y^{\pm}$.

$$A_{LU} = \frac{1}{P}\left(\frac{Y^+ - Y^-}{Y^+ + Y^-}\right), \delta_{\rm stat} = \frac{2}{P}\sqrt{\frac{Y^+Y^-}{(Y^+ + Y^-)^3}} \qquad (2)$$

$A_{LU}$ has been previously measured above the resonance region at Jefferson Lab Hall B in exclusive $\pi^+$ production [20, 21], and in exclusive $\pi^0$ [22]. This work reports the first measurement of $A_{LU}$ in $p(\vec{e}, e'\pi^+)n$ from Hall C as part of the KaonLT experiment, with significantly finer kinematic binning and cleaner identification of the exclusive final state compared to previous measurements of this observable.

A continuous wave electron beam with energy 10.585 GeV and beam current up to 70 $\mu$A was used. The beam energy was determined to ±3.6 MeV by measuring the bend angle of the beam into Hall C, as it traversed a set of dipole magnets with precisely calibrated field integrals [23]. The beam helicity was flipped at a frequency of 30 Hz in a pseudo-random sequence, with a **helicity-correlated** charge asymmetry of up to 0.1% [24]. No dedicated beam polarization measurements were made in Hall C. Rather, Mott polarimetry measurements were taken at the injector to the accelerator (90 ± 1%) [25], and a calculation of the spin precession through the accelerator indicated that for this beam energy Hall C receives 99% of the source polarization. These gave a result of $89^{+1}_{-3}\%$ longitudinal beam polarization to Hall C, where the uncertainty is determined from the beam energy uncertainty and the range of possible linac energy imbalance.

The electrons were incident upon a 10 cm (762 mg/cm$^2$) cryogenic unpolarized liquid hydrogen target. Two aluminum foils placed 10 cm apart were used **as a separate target setup, and a comparable amount of data was collected** for subtraction of the background from the aluminum end caps of the hydrogen target cell. Beam quality was assured by continuous measurements from three beam position monitors [26], four beam current monitors [27], and an Unser monitor [28].

**Charged pions were detected in the recently commissioned Super High Momentum Spectrometer (SHMS), which has momentum acceptance $\Delta p/p$ from -10 to +20% of the central momentum, and covers a solid angle of $\Delta\Omega$ = 4 msr [29]. The maximum SHMS central momentum is 11 GeV/c, and the central momentum is chosen to set the values ($Q^2$,$x_B$) for each experimental setting. Scattered electrons were detected in coincidence with the pions in the High Momentum Spectrometer (HMS), which has momentum acceptance $\Delta p/p$ = ±8%, solid angle $\Delta\Omega$ = 7 msr, and maximum central momentum 7 GeV/c [30].** Both spectrometers include two drift chambers for track reconstruction, hodoscope arrays for triggering, threshold Cherenkov detectors and lead-glass calorimeters for particle identification. Positive pions were identified in the SHMS using an aerogel Cherenkov detector with refractive index $n$ = 1.015 (for $p_\pi$ < 5 GeV/c) or $n$ = 1.011 (for $p_\pi$ > 5 GeV/c), for a pion detection efficiency of 97%. Electrons were identified in the HMS via a gas Cherenkov detector filled with $C_4F_{10}$ at 0.48 atm (refractive index 1.0008) in combination with the lead-glass calorimeter. Any remaining contamination from real $e-p$ and $e-K^+$ coincidences was eliminated with a coincidence time cut of ±2.25 ns and a missing mass cut of 0.91 < $m_x$ <1.01 GeV (Fig. 3). For the $p(\vec{e}, e'\pi^+)n$ reaction, the reconstructed missing mass $m_x^2 = (m_p + p_e - p_{e'} - p_\pi)^2$ is close to the free neutron mass, **with a radiative tail extending to higher $m_x$ (Fig. 3). The upper cut on the missing mass was selected to include as much of the radiative tail as possible without including contamination from $e-K^+$ events or Semi-Inclusive Deep Inelastic Scattering (SIDIS), which begins at $m_x$ = 1.05 GeV. No radiative corrections were applied to these data.**

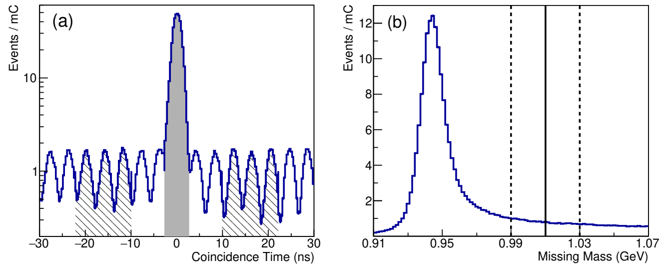


Figure 3: Coincidence time and missing mass spectra for Q$^2$=3.0 GeV$^2$, $x_B$=0.25, center SHMS setting. (a) Coincidence time between the HMS and SHMS. The prompt peak selected is highlighted in grey, and the windows used to subtract random coincidences are hatched. (b) Missing mass distribution of $p(\vec{e}, e'\pi^+)n$. The solid line shows the upper missing mass cut used, and the dashed lines show the variation of the cut used to calculate a cut dependence. The lower missing mass cut is 0.91 GeV, and its contribution to the cut dependence is evaluated by removing this cut entirely.

Background from aluminum target cell walls (1–2% of events) and random coincidences (∼3% of events at $x_B$=0.4 and ∼12% at $x_B$=0.25) were subtracted from charge normalized event yields. As the detector inefficiencies and data acquisition livetimes are uncorrelated with the electron beam helicity, they are expected to cancel in the calculation of $A_{LU}$ (Eqn. 2).

The ($Q^2$, $x_B$) settings studied in this experiment are shown in Fig. 4. For each ($Q^2$, $x_B$) setting, the HMS angle and momentum, as well as the SHMS momentum, were kept fixed. To attain full coverage in $\phi$, data were taken with the SHMS at ±3° of the $\vec{q}$-vector direction (virtual photon momentum), in addi-

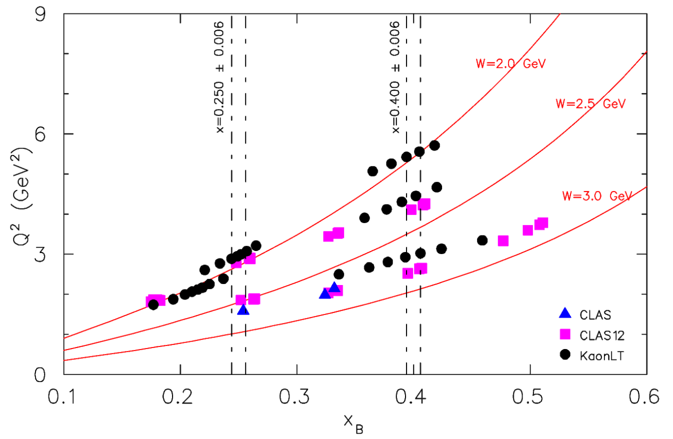


Figure 4: (Color online) Phase space plot of the kinematics for which $\sigma_{LT'}/\sigma_0$ has been measured [21, 20] [This work]. Only data with $-t < 0.7$ GeV$^2$ are shown. By combining these data sets, the $Q^2$ dependence of $\sigma_{LT'}/\sigma_0$ can be determined at fixed $x_B$ and $-t$ at two values of $x_B$, shown as dashed lines.

tion to data centered on the $\vec{q}$-vector (center setting).

The relevant kinematic variables, $Q^2$, $x_B$, $W$, and $t$ were reconstructed from the measured spectrometer quantities. **Using proton-electron elastic scattering (where the proton is detected in the SHMS and the electron in the HMS) as an overdetermined reaction,** the beam momentum and the spectrometer central momenta were determined absolutely to $< 0.5\%$, while the incident beam angle and spectrometer central angles were absolutely determined to $< 0.5$ mrad (method described in [31]).

For each ($Q^2$, $x_B$) setting, the data were split into 5—8 bins in $t$ and 15 bins in $\phi$, with the number of $t$-bins determined by the raw number of events at each setting. The asymmetry was calculated according to Eqn. 2 for each $t$-bin at each of the three SHMS angles. An error-weighted average was then taken to obtain a complete $\phi$ distribution. Fig. 5 shows the binned asymmetry for central kinematics of $Q^2$=3 GeV$^2$, $x_B$=0.25 for illustration. In exclusive pion production, the experimental acceptances in $x_B$, $Q^2$ and $t$ are correlated. Thus, for each $t$-bin (but independent of $\phi$), the mean $Q^2$ and $x_B$ values of the data vary slightly from the 'central' values.

Previous work assumed that $\sigma_{TT}/\sigma_0 \ll 1$ and $\sigma_{LT}/\sigma_0 \ll 1$, such that Eqn. 1 simplifies to $A_{LU} = A_{LU}^{\sin\phi} \sin\phi$, the justification being that the full functional form and the approximated form gave extremely similar results for $A_{LU}^{\sin\phi}$ [21, 20]. Neglecting $\sigma_{LT}/\sigma_0$ and $\sigma_{TT}/\sigma_0$ appears to be a low $-t$ approximation, which is insufficiently accurate for our fits at higher $-t$, as seen in the last panel of Fig. 5. The authors are aware of no theoretical constraints for why $\sigma_{LT}/\sigma_0$ and $\sigma_{TT}/\sigma_0$ should be negligible. **Additionally, a Monte Carlo study was performed which determined that at the experimental precision, it is not feasible to accurately determine if $\sigma_{LT}/\sigma_0$ and $\sigma_{TT}/\sigma_0$ are negligible.** Therefore, $A_{LU}^{\sin\phi}$ was determined using Eqn. 1, with $\sigma_{LT}/\sigma_0$ and $\sigma_{TT}/\sigma_0$ left as free parameters in the fit. The statistical error on $A_{LU}^{\sin\phi}$ is taken as the error of fitting when including the statistical uncertainties per $\phi$ bin. The cross section ratio $\sigma_{LT'}/\sigma_0$ and its statistical uncertainty were then extracted from $A_{LU}^{\sin\phi}$.

There were three main sources of systematic uncertainty. First is the difference in $\sigma_{LT'}/\sigma_0$ obtained using Eqn. 1 and the approximated fit. Since such a difference is unidirectional, the total systematic error (obtained from the quadrature sum of systematic uncertainties) is asymmetric, denoted $\delta_{\rm sys}^{\uparrow}$ and $\delta_{\rm sys}^{\downarrow}$ for the upper and lower error bars. This is the dominant systematic, contributing an average error of 12%, but up to 70%. Additionally, the uncertainty on the beam polarization contributed an uncertainty of 3.4%, and the dependence of $\sigma_{LT'}/\sigma_0$ on the exact values used in the coincidence time and missing mass cuts contributed between 1–7%, with one outlier at 12%.

## 3. Comparison with theoretical expectations

Fig. 6 shows $\sigma_{LT'}/\sigma_0$ compared to theoretical predictions. **The model calculations were evaluated at the mean $Q^2$ and $x_B$ of each panel in Fig. 6, whereas the true $Q^2$ and $x_B$ vary slightly across each $-t$ bin (see the supplemental material). This means that $(-t)_{\rm min}$ differs slightly between data and theory.**

Three distinct models were considered, of which one is based on the GPD formalism, and two on Regge trajectories. The Goloskokov-Kroll (GK) model [3, 18] calculates $\sigma_{LT'}$ for deep exclusive $\pi^+$ production in terms of the twist-2 longitudinal $(\widetilde{E}, \widetilde{H})$ and twist-3 transverse $(E_T, H_T)$ GPDs, with pion pole contributions. The default version of the GK model, denoted GK1, shows better agreement for $x_B = 0.40$ than for $x_B = 0.25$, in which case its $t$-dependence does not match the data. In Ref. [21], the argument was made that increasing the GPD $H_T$ in the GK calculation resulted in better agreement with experimental data. In this work, the curve GK2 is the GK model with the modification $H_T \to H_T * 2$. GK2 has a lower magnitude than GK1, bringing it closer to data, but it still does not re-create the $t$-dependence of $\sigma_{LT'}/\sigma_0$ properly at all kinematics.

Second, the Vrancx-Ryckebush (VR) model [19] considers Reggeized $\pi(140)$, $\rho(770)$, and $a_1(1260)$ exchanges. Including only $\pi(140)$ and $\rho(770)$ leads to a vanishing $A_{LU}$. The inclusion of the axial-vector $a_1(1260)$ exchange generates a nonzero $A_{LU}$ through interference with the vector $\rho(770)$ exchange [34]. However, this interference is still insufficient to reproduce $A_{LU}$ from previous CLAS data [35] without proper treatment of the "resonant effect" caused by nucleon form factors. For this work, the VR model agrees with the data reasonably well at low $-t$, but does not capture the plateau of $\sigma_{LT'}/\sigma_0$ that occurs at higher $-t$.

Finally, the Yu-Choi-Kong (YCK) model predicts $A_{LU}$ using Regge propagators, with contribution of the magnetic moment term of the nucleon with the Pauli form factor $F_2(Q^2)$. It incorporates the exchange of tensor meson $a_2(1320)$ with axial mesons $a_1$ and $b_1(1235)$, which were not included in the earlier version [36]. In the new model, the electromagnetic form factors (EMFFs) of the nucleon are considered in two categories: the GPD-mediated form [37], designated YCK1, and the typical dipole form, designated YCK2. The YCK model presents the best agreement with this work. YCK2 underestimates $\sigma_{LT'}/\sigma_0$,

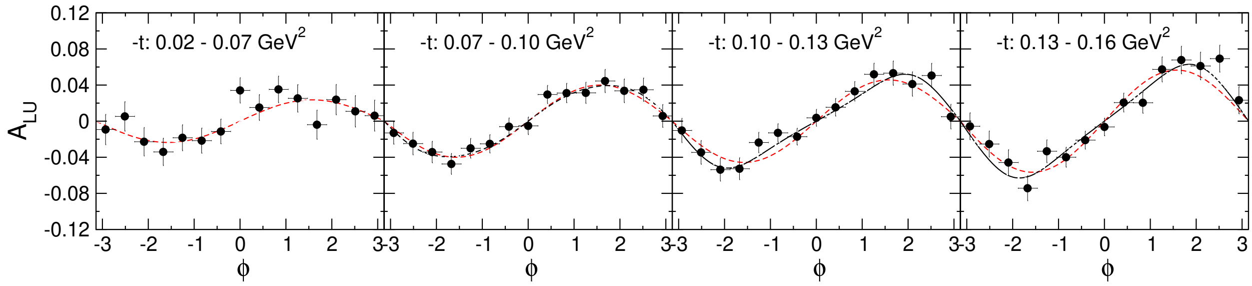


Figure 5: $A_{LU}$ as a function of $\phi$ for the first four $t$-bins for central values of $Q^2 = 3$ GeV$^2$, $x_B$ =0.25. The solid line shows the full fit and the dashed line the approximated fit (see text for explanation). Uncertainties are statistical only.

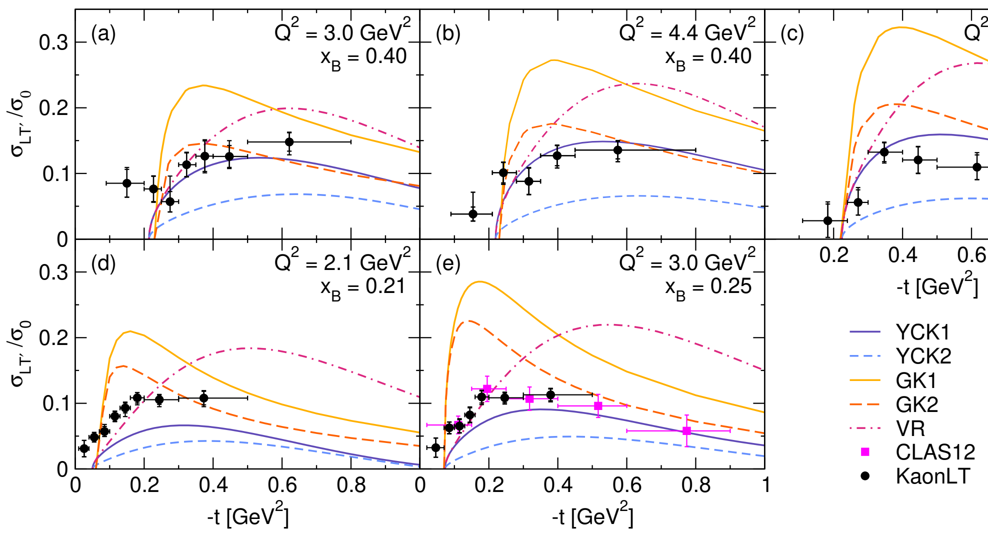


Figure 6: (Color online) The extracted $\sigma_{LT'}/\sigma_0$ as a function of $-t$ for each $(Q^2, x_B)$ setting. The horizontal error bar indicates the width of the $t$-bin, and the double vertical error bar shows the statistical and total errors. Exact values of $\sigma_{LT'}/\sigma_0$ and its uncertainties, as well as binned kinematics, are available in the supplemental material [32]. The smooth curves represent theory predictions (see legend) evaluated at the listed kinematics. GK1 refers to the default GK version [33], and GK2 is the GK model with the modification of $H_T \to H_T * 2$, following the example of Ref. [21]. YCK1 is the YCK model with the nucleon EMFFs parametrized with GPDs, whereas YCK2 uses a dipole parametrization. CLAS12 data [21] with comparable kinematics ($Q^2$ = 2.9 GeV$^2$, $x_B$=0.26) are included in panel (e).

but YCK1 provides a reasonable prediction of both the magnitude and $t$-dependence of $\sigma_{LT'}/\sigma_0$.

**Quantitatively, YCK1 has the lowest average $\chi^2$/NDF, although none of the calculated $\chi^2$/NDF values are close to 1. The VR model has the second-lowest $\chi^2$/NDF, but this is artificially influenced by the majority of data points being at low $-t$, before the VR model clearly diverges from the data. Overall, the Regge models outperform the GPD model, implying that these kinematics are not yet in the factorization regime, however it should be noted that this conclusion is model-dependant, and that no model completely predicts the data.**

## 4. Dependence of $\sigma_{LT'}/\sigma_0$ on Q$^2$

These results are in good agreement with recent results from CLAS12, showing a similar magnitude and $t$-dependence of $\sigma_{LT'}/\sigma_0$ [21]. At points with very similar $Q^2$, $x_B$ and $t$, the KaonLT and CLAS12 measurements agree within the quoted uncertainties. Furthermore, by comparing data between CLAS, CLAS12, and this work, two kinematic ranges were identified

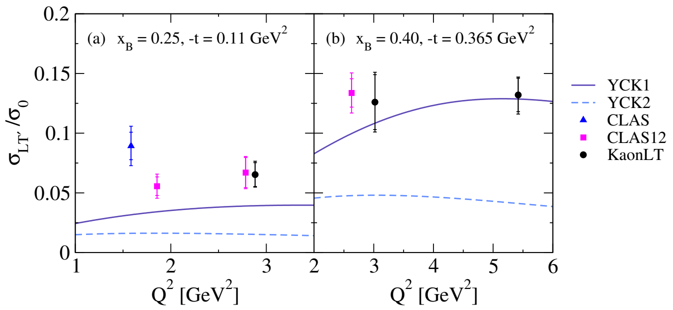


Figure 7: (Color online) Values of $\sigma_{LT'}/\sigma_0$ from three experiments [21, 20] [This work] plotted as a function of $Q^2$ at fixed $x_B$ and $-t$. The $Q^2$-dependence of the data is consistent, within error, with a horizontal line.

where it was possible to hold $x_B$ and $t$ **essentially** constant while varying $Q^2$, allowing the $Q^2$-dependence of $\sigma_{LT'}/\sigma_0$ to be determined (Fig. 7). At the two $(x_B, t)$ points investigated, **($x_B$ = 0.400 ± 0.006, $-t$ = 0.360 ± 0.016) and ($x_B$ = 0.250 ± 0.006, $-t$ = 0.112 ± 0.004),** the asymmetry is largely independent of $Q^2$. In Fig. 6, it can be seen that most theory curves incorporate a $Q^2$-dependence, in which the magnitude of the predicted $\sigma_{LT'}/\sigma_0$ increases with $Q^2$. This work suggests that in this regime, a description involving a significant $Q^2$-dependence is not entirely accurate. Future measurements of $\sigma_{LT'}/\sigma_0$ over a wider range of $Q^2$ would be beneficial to further test these predictions. Data have been taken in Hall C (PionLT experiment, E12-19-006 [38]) which could be used for this analysis.

## 5. Discussion and Conclusions

**The recent CLAS12 measurement of $\sigma_{LT'}/\sigma_0$ [21] concluded that the GK2 model best described the data, ergo the data (which covered $Q^2$=1.8 to $Q^2$=5.5 GeV$^2$) were in the GPD factorization regime. With the more precise kinematics and finer binning at lower $-t$ afforded by the KaonLT data, as well as access to the new YCK model, we believe this conclusion to be premature. There is insufficient evidence to assume that GPDs can sufficiently describe polarized observables in $p(e, e'\pi^+)n$ at these kinematics. We suggest the extraction of GPDs from these data should be delayed until a model-independent test can be performed, for example a scaling study of Rosenbluth separated cross-sections. A previous scaling study of pion electroproduction up to $Q^2$=3.9 GeV$^2$ from the F$\pi$-2 Collaboration was inconclusive [39], but analysis is ongoing to perform this measurement with data from both the KaonLT (maximum $Q^2$=5.5 GeV$^2$ [10]) and PionLT (maximum $Q^2$=8.5 GeV$^2$ [38]) experiments.**

In summary, the observable $A_{LU}$ and the cross section ratio $\sigma_{LT'}/\sigma_0$ of the $p(\vec{e}, e'\pi^+)n$ reaction have been measured at Hall C of Jefferson Lab over a wide range of kinematics. The dependence of $\sigma_{LT'}/\sigma_0$ on $-t$ at fixed $Q^2$ and $x_B$ was explored and compared to theoretical calculations. The best agreement is with YCK1, a Regge model in which the nucleon EMFFs are parametrized with GPDs. Additionally, the data are consistent with a flat or weak $Q^2$-dependence at fixed $x_B$ and $-t$. **In addition to a factorization scaling study of $p(e, e'\pi^+)n$,** future work with KaonLT data will include measurements of $\sigma_{LT'}/\sigma_0$ in $p(e, e'\pi^+)\Delta^0$ and $u$-channel meson production, **and Rosenbluth separated cross-sections for $p(e, e'K^+)\Lambda/\Sigma$.**


## Acknowledgements

We thank the staff of the Accelerator and the Physics Divisions at Jefferson Lab for their excellent efforts during the experimental data taking. This material is based upon work supported by the U.S. Department of Energy, Office of Science, Office of Nuclear Physics under contract DE-AC05-06OR23177. This work is supported by the Natural Sciences and Engineering Research Council of Canada (NSERC) SAPIN-2021-00026 and a Canadian Institute of Nuclear Physics graduate fellowship. Additional support is gratefully acknowledged from: the University of Regina, the U.S. National Science Foundation (NSF) grants PHY 2309976, 2012430 and 1714133 at the Catholic University of America, NSF grant PHY 2209199 at Ohio University, UK Science and Technology Facilities Council (STFC) grant ST/W004852/1 at the University of York, and National Research Foundation of Korea (NRF) grant NRF-2022 R1A2B5B01002307.


## References


[1] A. V. Radyushkin, Asymmetric gluon distributions and hard diffractive electroproduction, Phys. Lett. B 385 (1996) 333–342. doi:10.1016/0370-2693(96)00844-1.

[2] J. C. Collins, L. Frankfurt, M. Strikman, Factorization for hard exclusive electroproduction of mesons in QCD, Phys. Rev. D 56 (1997) 2982–3006. doi:10.1103/PhysRevD.56.2982.
URL https://link.aps.org/doi/10.1103/PhysRevD.56.2982

[3] S. V. Goloskokov, P. Kroll, An attempt to understand exclusive $\pi^+$ electroproduction, Eur. Phys. J. C 65 (1-2) (2009).
URL https://doi.org/10.1140/epjc/s10052-009-1178-9

[4] C. Muñoz Camacho, et al., Scaling tests of the cross section for deeply virtual compton scattering, Phys. Rev. Lett. 97 (2006) 262002. doi:10.1103/PhysRevLett.97.262002.
URL https://link.aps.org/doi/10.1103/PhysRevLett.97.262002

[5] F. X. Girod, et al., Measurement of deeply virtual compton scattering beam-spin asymmetries, Phys. Rev. Lett. 100 (2008) 162002. doi:10.1103/PhysRevLett.100.162002.
URL https://link.aps.org/doi/10.1103/PhysRevLett.100.162002

[6] Favart, L., Guidal, M., Horn, T., Kroll, P., Deeply virtual meson production on the nucleon, Eur. Phys. J. A 52 (6) (2016) 158. doi:10.1140/epja/i2016-16158-2.
URL https://doi.org/10.1140/epja/i2016-16158-2

[7] D. Müller, Generalized parton distributions: Visions, basics, and realities, Few-Body Syst. 55 (5-7) (2014) 317–337. doi:10.1007/s00601-014-0894-3.
URL https://doi.org/10.1007%2Fs00601-014-0894-3

[8] M. Diehl, Generalized parton distributions, Phys. Rep. 388 (2-4) (2003) 41–277. doi:10.1016/j.physrep.2003.08.002.
URL https://doi.org/10.1016%2Fj.physrep.2003.08.002

[9] G. R. Goldstein, J. O. G. Hernandez, S. Liuti, Flexible parametrization of generalized parton distributions: The chiral-odd sector, Phys. Rev. D 91 (2015) 114013. doi:10.1103/PhysRevD.91.114013.
URL https://link.aps.org/doi/10.1103/PhysRevD.91.114013

[10] T. Horn, G. M. Huber, P. Markowitz, et al., Studies of the L/T Separated Kaon Electroproduction Cross Sections from 5-11 GeV, Jefferson Lab 12 GeV Experiment E12-09-011 (2008).
URL https://www.jlab.org/exp_prog/proposals/proposal_updates/E12-09-011_Update_pac38.pdf

[11] M. Diehl, S. Sapeta, On the analysis of lepton scattering on longitudinally or transversely polarized protons, Eur. Phys. J. C 41 (4) (2005) 515–533. doi:10.1140/epjc/s2005-02242-9.
URL http://dx.doi.org/10.1140/epjc/s2005-02242-9

[12] T. Arens, O. Nachtmann, M. Diehl, P. V. Landshoff, Some tests for the helicity structure of the pomeron in e p collisions, Z. Phys. C 74 (1997) 651–669. doi:10.1007/s002880050430.

[13] A. Bacchetta, U. D'Alesio, M. Diehl, A. Miller, Single-spin asymmetries: The trento conventions, Phys. Rev. D 70 (10 2004). doi:10.1103/PhysRevD.70.117504.

[14] T. Regge, Introduction to complex orbital momenta, Nuovo Cim 14 (1959) 951–976. doi:https://doi.org/10.1007.

[15] B. G. Yu, T. K. Choi, W. Kim, Regge phenomenology of pion photoproduction off the nucleon at forward angles, Phys. Rev. C 83 (2011) 025208.
URL https://api.semanticscholar.org/CorpusID:119117429

[16] J. Laget, Exclusive meson photo- and electro-production, a window on the structure of hadronic matter, Prog. Part. Nucl. Phys. 111 (2020) 103737. doi:10.1016/j.ppnp.2019.103737.
URL http://dx.doi.org/10.1016/j.ppnp.2019.103737

[17] G. M. Huber, et al., Charged pion form factor between $Q^2$=0.60 and 2.45 GeV$^2$. II. Determination of, and results for, the pion form factor, Phys. Rev. C 78 (2008) 045203. doi:10.1103/PhysRevC.78.045203.
URL https://link.aps.org/doi/10.1103/PhysRevC.78.045203

[18] S. V. Goloskokov, P. Kroll, Transversity in hard exclusive electroproduction of pseudoscalar mesons, Eur. Phys. J. A 47 (2011) 112. doi:10.1140/epja/i2011-11112-6.
URL https://doi.org/10.1140/epja/i2011-11112-6

[19] T. Vrancx, J. Ryckebusch, Charged pion electroproduction above the resonance region, Phys. Rev. C 89 (2) (2014) 025203. doi:10.1103/PhysRevC.89.025203.

[20] S. Diehl, et al., Extraction of beam-spin asymmetries from the hard exclusive $\pi^+$ channel off protons in a wide range of kinematics, Phys. Rev. Lett. 125 (2020) 182001. doi:10.1103/PhysRevLett.125.182001.
URL https://link.aps.org/doi/10.1103/PhysRevLett.125.182001

[21] S. Diehl, et al., A multidimensional study of the structure function ratio $\sigma_{LT'}/\sigma_0$ from hard exclusive $\pi^+$ electro-production off protons in the GPD regime, Phys. Lett. B 839 (2023) 137761. doi:https://doi.org/10.1016/j.physletb.2023.137761.
URL https://www.sciencedirect.com/science/article/pii/S0370269323000953

[22] R. De Masi, et al., Measurement of $ep \to ep\pi^0$ beam spin asymmetries above the resonance region, Phys. Rev. C 77 (2008) 042201. doi:10.1103/PhysRevC.77.042201.
URL https://link.aps.org/doi/10.1103/PhysRevC.77.042201

[23] D. W. Higinbotham, Using Polarimetry To Determine The CEBAF Beam Energy, PoS Proc. Sci. PSTP2013 (2013) 014. doi:10.22323/1.182.0014.

[24] J. Benesch, A. Bogacz, A. Freyberger, Y. Roblin, T. Satogata, R. Suleiman, M. Tiefenback, 12 gev cebaf beam parameter tables, Tech. rep., Jefferson Laboratory, JLAB-TN-18-022 (2018).

[25] J. M. Grames, et al., High precision 5 MeV Mott polarimeter, Phys. Rev. C 102 (2020) 015501. doi:10.1103/PhysRevC.102.015501.
URL https://link.aps.org/doi/10.1103/PhysRevC.102.015501

[26] J. Benesch, et al., Jefferson Lab Hall C: Precision Physics at the Luminosity Frontier (2022). arXiv:2209.11838.

[27] D. J. Mack, Beam current monitors for Hall C, AIP Conf. Proc. 269 (1) (1992) 527–530. doi:10.1063/1.42965.
URL https://doi.org/10.1063/1.42965

[28] K. B. Unser, The parametric current transformer, a beam current monitor developed for LEP, AIP Conf. Proc. 252 (1) (1992) 266–275. doi:10.1063/1.42124.
URL https://doi.org/10.1063/1.42124

[29] S. Ali, et al., The SHMS 11 GeV/c Spectrometer in Hall C at Jefferson Lab, to be published (2024).

[30] H. P. Blok, et al., Charged pion form factor between $Q^2 = 0.60$ and 2.45 GeV$^2$. I. Measurements of the cross section for the $^1$H$(e, e^{'}\pi^+)n$ reaction, Phys. Rev. C 78 (2008) 045202. doi:10.1103/PhysRevC.78.045202.
URL https://link.aps.org/doi/10.1103/PhysRevC.78.045202

[31] J. Volmer, The Pion Charge Form Factor via Pion Electroroduction on the Proton, PhD Thesis, Vrije Universiteit te Amsterdam (2000).
URL https://misportal.jlab.org/ul/publications/view_pub.cfm?pub_id=5412

[32] See Supplemental Material at [URL will be inserted by publisher] for tabulated values of kinematics, $\sigma_{LT'}/\sigma_0$ and uncertainties. [link].
URL TBA

[33] B. Berthou, D. Binosi, N. Chouika, M. Guidal, C. Mezrag, H. Moutarde, F. Sabatié, P. Sznajder, J. Wagner, PARTONS: PARtonic Tomography Of Nucleon Software. A computing platform for the phenomenology of Generalized Parton Distributions, Eur. Phys. J. C 78 (12 2015). doi:10.1140/epjc/s10052-018-5948-0.

[34] M. M. Kaskulov, U. Mosel, Deep exclusive charged $\pi$ electroproduction above the resonance region, Phys. Rev. C 81 (2010) 045202. doi:10.1103/PhysRevC.81.045202.
URL https://link.aps.org/doi/10.1103/PhysRevC.81.045202

[35] H. Avakian, L. Elouadrhiri, Single spin asymmetries at CLAS, Phys. Part. Nucl. 35 (2004) S114–S120.

[36] T. K. Choi, K. J. Kong, B. G. Yu, Pion and proton form factors in the regge description of electroproduction $p(e, e'\pi^+)n$, J. Korean Phys. Soc. 67 (7) (2015) 1089–1094. doi:10.3938/jkps.67.1089.
URL http://dx.doi.org/10.3938/jkps.67.1089

[37] M. Guidal, M. V. Polyakov, A. V. Radyushkin, M. Vanderhaeghen, Nucleon form factors from generalized parton distributions, Phys. Rev. D 72 (2005) 054013. doi:10.1103/PhysRevD.72.054013.
URL https://link.aps.org/doi/10.1103/PhysRevD.72.054013

[38] D. Gaskell, T. Horn, G. M. Huber, et al., Study of the L–T Separated Pion Electroproduction Cross Section at 11 GeV and Measurement of the Charged Pion Form Factor to High Q$^2$, Jefferson Lab 12 GeV Experiment E12-19-006 (2009).
URL https://www.jlab.org/exp_prog/proposals/19/E12-19-006.pdf

[39] T. Horn, et al., Scaling study of the pion electroproduction cross sections, Phys. Rev. C 78 (5) (2008) 058201. doi:10.1103/physrevc.78.058201.
URL http://dx.doi.org/10.1103/PhysRevC.78.058201